

Scaling of a long-range interacting quantum spin system driven out of equilibrium

S. Helmrich,¹ A. Arias,¹ and S. Whitlock¹

¹*Physikalisches Institut, Universität Heidelberg, Im Neuenheimer Feld 226, 69120 Heidelberg, Germany.*

(Dated: August 4, 2016)

Complex systems are often found to exhibit unexpectedly simple scaling laws that can signal new physical regimes or universal relations between otherwise very different systems. Although this provides a powerful tool for characterising systems close to equilibrium, there are only few known examples where scaling behaviour can be found in dynamical settings. Here we demonstrate power-law scaling in a well-controlled quantum spin system driven out of equilibrium. This enables us to reconstruct the non-equilibrium phase diagram of the system and identify dissipation-dominated, driving-dominated and interaction-dominated regimes. The measured scaling laws show signatures of the underlying ground state phase structure, including paramagnetic behaviour, quantum critical behaviour and a magnetic instability towards states with strong spatial correlations. This opens up a new means to study and classify quantum systems out of equilibrium and extends the domain where scale-invariant behaviour can be found.

Throughout nature and society, complex systems are found to exhibit surprisingly simple scaling laws that arise due to subtle correlations in the system [1]. A seminal example is the transition between paramagnetic and ferromagnetic phases of Ising magnets and the liquid-gas transition in fluids [2]. Close to their respective transition points, macroscopic observables of both systems can be completely characterised by power-laws involving a few common scaling exponents indicative of a shared universality class. Thus scaling laws offer a powerful way to reveal common or distinguishing characteristics of seemingly very different states of matter.

While the utility of scaling laws has been clearly established for systems close to equilibrium, there are still relatively few examples where they are known to apply in out of equilibrium scenarios [3]. This is especially relevant for a new generation of experiments which aim to probe exotic forms of quantum matter, ranging from laser cooled ion crystals [4–6] and optically driven quantum gases [7–10], to semiconductor exciton-polariton condensates [11] and superconducting circuits [12]. In each of these experiments a quantum many-body system is brought out of equilibrium, either, by a sudden change of system parameters, or by continuous driving with external fields to short-lived excited states. This often results in dissipation (e.g., due to spontaneous decay) leading to an interplay between coherent and incoherent dynamics. Combined with strong interactions between the particles, a rich variety of new regimes and complex types of behaviour can emerge that are quite distinct from the properties of the ground state and have no counterparts in traditional condensed-matter physics. This poses a significant challenge to state-of-the-art many-body theory and experiments, in part because theoretical methods capable of dealing with non-equilibrium problems are less developed, and because it is difficult to devise observables capable of distinguishing the vastly different types of behaviour they exhibit.

Here we report the out-of-equilibrium dynamics of a widely tunable driven-dissipative quantum spin system following a sudden quench of the system parameters. We

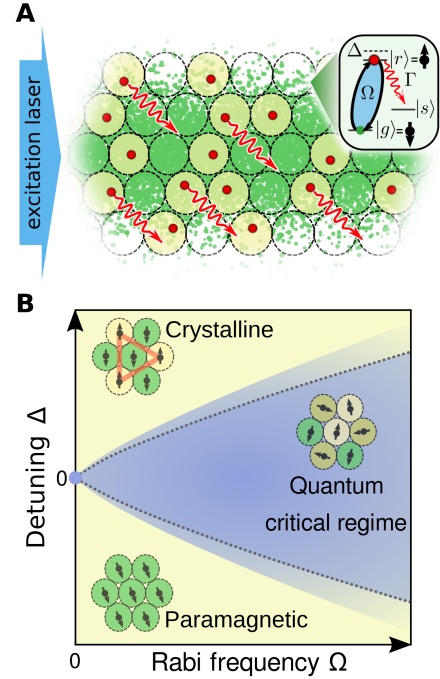


Figure 1. Platform for studying out of equilibrium dynamics of a long-range interacting quantum spin system. (A) Geometry of the atomic gas (green dots) driven to highly excited Rydberg states (red dots) by a laser. The ground and Rydberg states of each atom form a pseudospin-1/2 in transverse (Ω) and longitudinal (Δ) fields. The black dashed circles represent the characteristic blockade volume, within which the number of Rydberg excitations is limited to at most one. Spontaneous decay of the Rydberg state populates the shelving state $|s\rangle$. (B) Sketch of the anticipated ground state phase diagram showing paramagnetic, crystalline and quantum critical phases, with the quantum critical point at $\Omega = 0$ and $\Delta = 0$.

discover that the rate of population loss due to the decay of excited states provides a convenient macroscopic observable that exhibits power law scaling over a wide range of parameters. This enables the identification of dissipation-

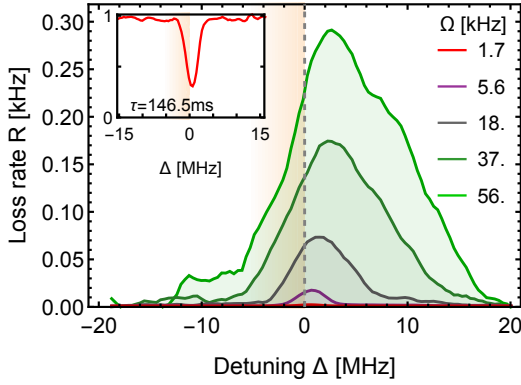


Figure 2. **Measured loss rates as a function of detuning Δ for various driving field strengths Ω .** For increasing Ω the spectra become asymmetric and broaden. The orange shaded region illustrates the range of detunings corresponding to the two-photon resonance accounting for inhomogeneous light shifts of the optical trap. **Inset:** Fraction of atoms $P(\tau)/P(0)$ remaining in $|g\rangle$ for $\Omega = 1.7$ kHz.

dominated, driving-dominated and interaction-dominated regimes in a single experimental system, as well as the mapping of its corresponding non-equilibrium ‘phase diagram’.

Our experimental system consists of an ultracold atomic gas coherently driven to states involving a small fraction of Rydberg excitations (Fig. 1A). By associating the ground and Rydberg states with a pseudospin-1/2 the system can be mapped to a quantum Ising model [13–15]. Ising-like spin-spin interactions originate from the van der Waals interactions between Rydberg states (falling off as a power law C_6/r^6). These interactions extend far beyond nearest neighbours such that a single excitation can suppress the subsequent excitation of hundreds of nearby spins within a characteristic blockade volume. Additionally, the single-atom atom-light coupling strength Ω and detuning from the atomic transition Δ play the roles of transverse and longitudinal magnetic fields, respectively. The resulting ground state phase diagram (Fig. 1B) includes a paramagnetic phase and a hierarchy of crystalline phases with varying excitation density [14]. For finite Ω these phases are separated by an experimentally accessible quantum critical region [16, 17]. Another feature of the system (which is usually neglected in quantum spin models) is the competition between coherent driving and spontaneous decay of the Rydberg states which can result in a crossover between coherent and incoherent dynamics similar to that of cavity quantum electrodynamics [7, 8].

The atomic gas consists of 7.5×10^4 ^{39}K atoms in the $|g\rangle = |4s_{1/2}, F=2, m_F=2\rangle$ state in a cigar shaped optical dipole trap with a peak density of $\rho = 1.1 \times 10^{11} \text{ cm}^{-3}$ and temperature $T = 19.4 \mu\text{K}$. All atoms in the sample are driven from $|g\rangle$ to $|r\rangle = |66s\rangle$ by a coherent two-photon laser excitation (see Methods) with large detuning from the intermediate state to minimise its population. We express the laser parameters in terms of the effective

two-photon Rabi frequency Ω , which we vary from 1.7 kHz to 56 kHz, and the detuning Δ which is varied over the range ± 20 MHz (Fig. 2). The effective decay rate including spontaneous emission from the short-lived intermediate state is $\Gamma \approx 100$ kHz. The number of atoms per blockade volume on resonance can be approximated by the solution to the self-consistent equation $N = \rho V_N$. Here ρ is the atomic density and $V_N = (4\pi/3)(C_6/\sqrt{N}\Omega)^{1/2}$ is the three-dimensional blockade volume, which depends on $\sqrt{N}\Omega$ due to the collectively enhanced atom-light coupling [18]. For the Rydberg state used, interactions are approximately isotropic and repulsive, with the van der Waals coefficient $C_6 = 270 \text{ GHz } \mu\text{m}^6$. For the maximum value of $\Omega = 56$ kHz this results in a minimum blockade volume $V_N = (4\pi/3)(8 \mu\text{m})^3$. Accounting for the inhomogeneous atomic distribution in the trap, the mean number of atoms per blockade volume is $\bar{N} \gtrsim 30$ [16].

To explore the out-of-equilibrium dynamics we start with all atoms initially prepared in the electronic ground state, i.e. the fully magnetised state with $\langle\sigma_z\rangle = -1$, where $\langle\sigma_z\rangle$ is the z-projection of the magnetisation. The driving field is then suddenly switched on with fixed values of Ω and Δ corresponding to different regions of the equilibrium phase diagram (Fig. 1B). Following this quench the system evolves towards states with a small fraction of Rydberg excitations. These excitations can then decay by spontaneous emission, either back to the ground state $|g\rangle$ or to the auxiliary $|s\rangle = |4s_{1/2}, F=1\rangle$ shelving state, leading to a loss of population from the system with instantaneous rate $\frac{\Gamma}{2}(\langle\sigma_z\rangle + 1)$, thus providing a direct experimental probe of the many-body state of the system. After the system has evolved for a finite time τ (between 1.4 ms and 146.5 ms) we switch off the driving field and measure the remaining fraction of ground state atoms $P(\tau)/P(0)$ using absorption imaging. This is then converted to a rate by assuming exponential decay $R = -(2\pi\tau)^{-1} \ln[P(\tau)/P(0)]$, although we verified that our results are not significantly affected by assuming a different time dependence. By adapting τ for each value of Ω to limit the maximum lost fraction to ≈ 0.5 (roughly the average time for each atom to decay once when driven on resonance) we achieve a dynamic range covering four orders of magnitude in loss rate spanning both coherent and incoherent evolution regimes.

The obtained loss-rate spectra (Fig. 2) show a strong dependence on driving strength and detuning. The maximal observed loss rate of 0.3 kHz is well below the expected upper limit for complete saturation of the Rydberg density $\Gamma/(2\bar{N}) = 1.6$ kHz. For the smallest Ω we observe a symmetric Gaussian lineshape with a full width half maximum of 3 MHz consistent with inhomogeneous broadening due to the dipole trap laser (see Supplementary Information). As Ω is increased, the resonance width grows and becomes noticeably asymmetric towards positive detunings which is a signature of the strong interparticle interactions.

Analysing the loss rate as a function of Ω for detunings below and above resonance we find the data are well described by power-law growth $R \propto \Omega^\alpha$ spanning several

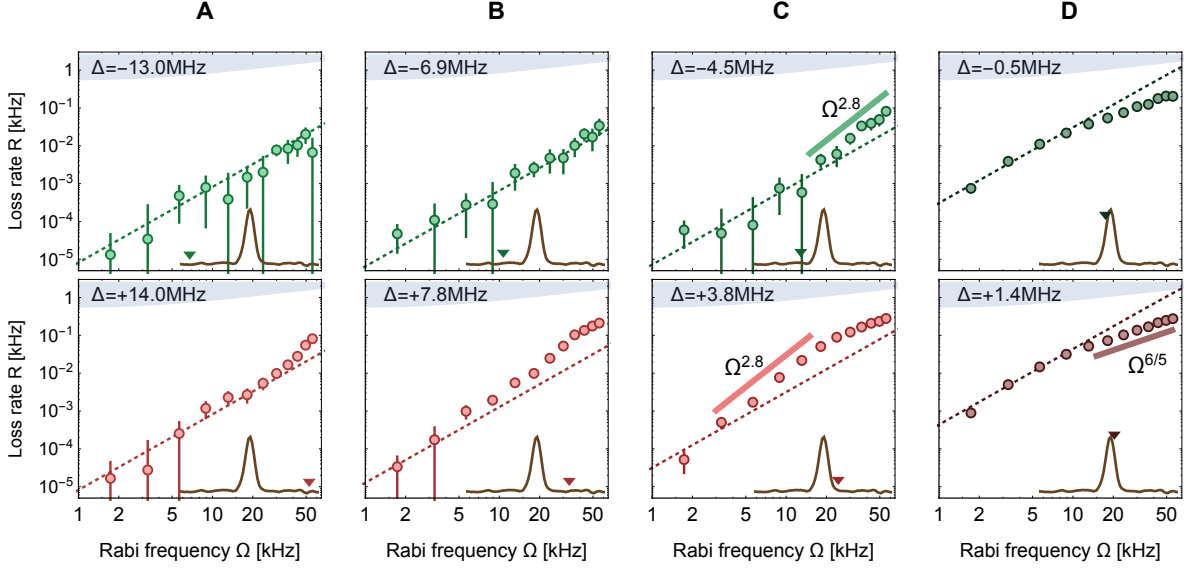


Figure 3. **Scaling of the loss rate as a function of driving strength.** The loss rate follows power-law scaling as a function of Ω with exponents which depend on the different regimes of the driven system. The dotted lines show the solution of the master equation in the non-interacting limit. (A) Far from resonance the loss rate follows a Ω^α scaling with $\alpha = 2$ expected for the paramagnetic (driving-dominated) regime. (B) and (C) For intermediate detunings and driving field strengths we observe a systematic change in slope reflecting an enhanced scaling exponent $\alpha > 2$ attributed to cooperative excitation processes. (D) Shows the crossover from the strongly-dissipative ($\alpha = 2$) to quantum critical regime. The gray curved area in each subfigure represents the upper limit to the loss rate $R = \Gamma/(2\bar{N})$ at full saturation. Errorbars correspond to the standard error of the mean over ten measurements.

orders of magnitude in R and Ω (Fig. 3). The exponents depend on the parameters of the driving field, indicating the existence of qualitatively different regimes.

Far below resonance and far above resonance the data are consistent with $\alpha \approx 2$ over most of the measurement range (Fig. 3A). This is characteristic of the driving dominated regime in which each spin precesses about the effective magnetic field and interactions are a small perturbation (see Supplementary Information). The expected loss rate given by the time-averaged magnetisation ($\langle \sigma_z \rangle = \Omega^2/(2\Delta^2) - 1$) is $R = \Omega^2/(4\Delta^2)$. This is equivalent to each atom being in the weakly-dressed state $|\psi\rangle = |g\rangle + \beta|r\rangle$ with $\beta = \Omega/(2\Delta) \ll 1$, which holds great promise for the realisation of new types of quantum fluids which exploit the novel interaction properties of Rydberg-dressed atoms [19–22].

Driving the system close to resonance (Fig. 3D) we observe power-law scaling with two distinct exponents separated by a sharp crossover. For large Ω the best fit exponent has a mean of $\alpha = 1.185$ and standard deviation of 0.025 for detunings in the range ± 1 MHz. This non-trivial scaling exponent is a signature of quantum critical behaviour in the interaction dominated regime. It is best understood for the special case $\Delta = \Gamma = 0$ which has been investigated in one experiment [17] and is amenable to theoretical treatment [13]. A simple model is to assume that the gas is comprised of a collection of superatoms, each with different N , which are driven coherently with

rate $\sqrt{N}\Omega$ [16]. Assuming van der Waals interactions in three-dimensions this yields a loss rate per atom $R \propto \Omega^{6/5}$, in accordance with universal scaling theory [17]. Our experiments confirm this scaling on resonance but also show that the influence of quantum criticality on non-equilibrium dynamics persists for a wide range of detunings away from resonance.

As the driving strength on resonance is reduced toward the quantum critical point at $(\Omega, \Delta) \rightarrow 0$, we observe a crossover to $\alpha = 2$ scaling at $\Omega_{\text{crit}} \approx 7$ kHz. This is consistent with the crossover from quantum-coherent to incoherent (dissipation dominated) dynamics governed by uncorrelated single-particle (de)excitation rates of the form $R \approx \Omega^2/\Gamma$. In the dissipative regime facilitated growth of correlated structures [23–26] and bistability [27, 28] has been observed, while theoretical work has identified analogies with soft-condensed matter systems [29–33] or wireless networks [34]. We directly see the crossover from coherent to dissipative dynamics, which interestingly does not occur for the simple criterion $\Omega \lesssim \Gamma$, but rather coherent effects persist for much weaker driving due to the collectively enhanced atom-light coupling. The measured position of the crossover is in good agreement with the critical driving strength $\Omega_{\text{crit}} = \Gamma/\sqrt{2\bar{N}} \approx 9$ kHz, which is analogous to the collective strong-coupling regime of cavity quantum electrodynamics [7, 8], illustrating the similarity between different driven-dissipative quantum systems.

For intermediate detunings we observe qualitatively new behaviour with stronger scaling compared to all other regimes (Fig. 3B, C). To test if it also follows a power-law scaling we fit the data to both algebraic and exponential growth models. For the data shown in Fig. 3C(lower panel) we obtain $\alpha = 2.81(9)$ with a reduced $\chi^2 = 0.63$ for the algebraic model which is favored over the exponential model with $\chi^2 = 11.3$. Power-law scaling is observed over a wide range of detunings above resonance ($\Delta \approx 7 \pm 3$ MHz) as well as a smaller range below resonance ($\Delta \approx -3.5 \pm 1.5$ MHz). Fitting the data over these ranges we find the scaling exponent varies by only about 10%. This scaling persists for driving field strengths well above the critical value for dissipative dynamics and cannot be explained by independent or incoherent excitations, suggesting that this is a qualitatively new regime.

We attribute this enhanced scaling behaviour to a magnetic instability associated to the crystalline ground state that causes the system to evolve toward many-body states with strong spatial correlations. Such instabilities can give rise to dynamical critical phenomena and scaling behaviour far from equilibrium [3]. A possible microscopic mechanism responsible for the observed scaling involves the cooperative excitation of distant atom pairs for detuned driving which matches the resonance condition $\Delta \approx C_6/(2r_{\text{pair}}^6)$. These spurious pair excitations can then act as nucleation sites for additional facilitated excitations at characteristic distances resulting in exponentially accelerated growth of the number of Rydberg excitations (previously demonstrated for dissipative dynamics [23–26, 35]). The same mechanism is also possible for a small range of detunings below resonance if one accounts for the inhomogeneous light shifts of the optical trap, c.f. Fig. 2(orange shaded region). While this mechanism is qualitatively compatible with our observations, it is yet to be seen if the precise value of the scaling exponent in the unstable regime can be reproduced in theory. Thus our experiments may serve as an exceptional benchmark for state-of-the-art theoretical methods for treating driven-dissipative many-body systems.

Finally, using scaling laws we map out the entire non-equilibrium phase diagram (Fig. 4). The scaling exponents as a function of Δ and Ω are obtained from the slopes of linear fits to $R(\Omega)$ in a moving window on a log-log scale. In contrast to the loss rate R , which is a smooth function with few distinguishing features (Fig. 4A), the scaling exponents show distinct regimes corresponding to the critical (blue) and unstable (red) scaling regimes (Fig. 4B). The strongly-dissipative regime appears as a mostly white region within the detuning interval $|\Delta| < 1$ MHz and for $\Omega \lesssim 7$ kHz. Moving to larger (positive) or negative detunings, we conclude that the system evolves into a (meta)stable paramagnetic state characterised by $\alpha \approx 2$ scaling. Despite the small signal-to-noise ratios in these two regimes we note that as the detuning is switched from negative to positive values a slight trend from blue-to-red is apparent, which might be due to weak interactions influencing the dynamics before entering

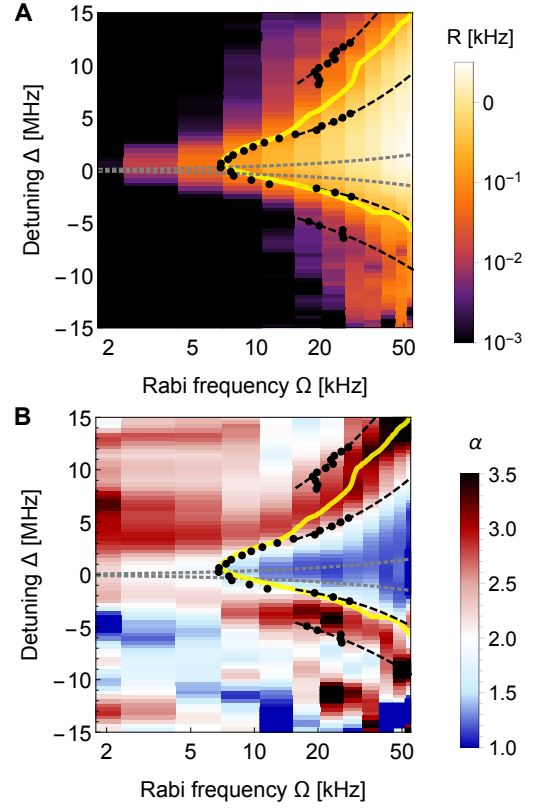


Figure 4. Experimentally measured phase diagram of the driven system. (A) As a function of the driving parameters the rate R is fairly smooth with few distinguishing features. (B) In contrast, the locally determined scaling exponent α shows clearly distinguished regimes. The quantum critical regime is identified as the blue region ($\alpha \approx 1.2$), while the superlinear regime is red ($\alpha > 2$). The gray dotted lines indicate the simple criteria $\bar{N}\beta^2 = 1$ for the critical regime [22] but stretched $10\times$ in the vertical scale for clarity. The black datapoints show the measured boundaries and the dashed black lines are power-law fits described in the text. The solid yellow line is the contour $\bar{N}(R/\Gamma) = 0.016$.

strongly-correlated phases.

To locate the boundaries between the regimes we fit piecewise linear functions to the log-scaled loss rates for each detuning. In addition to the quantum-critical to dissipative crossover, we identify four more boundaries which separate paramagnetic, unstable and quantum critical behaviour on both sides of the resonance. Each boundary follows a scaling $\Delta \propto \Omega^\gamma$ with $\gamma = \{0.69(7), 0.80(5), 0.6(2), 0.99(2)\}$ (dashed lines in Fig. 4 from top to bottom). This encompasses the theoretically predicted scaling for the boundary of the quantum-critical regime at equilibrium $\gamma = 4/5$ [22]. However, it is striking that the area of the quantum critical region is much larger than predicted by $\bar{N}\beta^2 \geq 1$ [22, 36]. This we attribute to the magnetic instability which acts as a catalyst, driving the system to the quantum critical regime over a wider range of detunings than expected without this instability (see also for example datapoints versus

dashed line in Fig. 3C). Instead, the boundary to the quantum critical regime is well reproduced by the experimentally determined criteria $\bar{N}(R/\Gamma) \geq \epsilon$ with $\epsilon \approx 0.016$ (yellow contour), where $R/\Gamma \sim \beta^2$ applies only in the paramagnetic regime.

We have demonstrated that scaling laws provide a convenient and powerful way to clearly identify vastly different regimes of driven-dissipative systems which can be applied in almost any experimental platform. The observed non-equilibrium scaling exponents reflect the underlying quantum phase structure and include signatures associated to paramagnetic, quantum critical and crystalline ground state phases. We also identify the boundary from coherent to incoherent dynamics governed by the collectively enhanced atom-light coupling. In the region corresponding to a crystalline ground state we observe new scaling behaviour attributed to a magnetic instability which drives the system towards strongly-correlated states.

Our results also shed light on the recent observation of anomalous broadening in weakly-dressed systems [37, 38]. In [37] for example, the almost linear dependence of the resonant scattering rate on Ω appears to be consistent with quantum critical scaling, indicating that these scaling laws are very robust with respect to different densities, interaction strengths or particle motion. Thus, scaling laws will serve as a powerful tool for identifying universal and non-universal aspects of non-equilibrium quantum systems and as a benchmark for future many-body theories. With recently developed high resolution imaging techniques for Rydberg atoms [39, 40], it will soon be possible to explore the topology underlying the observed scaling behaviour, including spatio-temporal correlations or possible self-similar characteristics.

ACKNOWLEDGMENTS

We acknowledge discussions with H. Weimer, S. Jochim and M. Weidemüller, as well as V. Ivannikov and E. Pavlov for contributions to the experimental setup. This work is supported by the Deutsche Forschungsgemeinschaft under WH141/1-1 and is part of and supported by the DFG Collaborative Research Centre "SFB 1225 (ISOQUANT)", the Heidelberg Center for Quantum Dynamics, the European Union H2020 FET Proactive project RySQ (grant N. 640378). S.H. acknowledges support by the Carl-Zeiss foundation, A.A. acknowledges support by the Heidelberg Graduate School for Fundamental Physics.

AUTHOR CONTRIBUTIONS

All authors made critical contributions to the work, discussed the results, and contributed to the writing of the manuscript.

AUTHOR INFORMATION

Correspondence and requests for materials should be addressed to S.W. (whitlock@uni-heidelberg.de).

METHODS

Coherent two-photon laser excitation

To couple the ground state $|g\rangle = |4s_{1/2}, F=2, m_F=2\rangle$ and the Rydberg state $|r\rangle = |66s\rangle$ we use a coherent two-photon excitation scheme. This utilises a weak ‘probe’ laser at 767 nm wavelength for the $|g\rangle \leftrightarrow |e\rangle = |4p_{3/2}\rangle$ transition and a strong ‘coupling’ laser at 456 nm wavelength for the $|e\rangle \leftrightarrow |r\rangle$ transition. The atomic cloud has $e^{-1/2}$ radii $\{\sigma_r, \sigma_z\} = \{14 \mu\text{m}, 220 \mu\text{m}\}$. The probe laser is aligned perpendicularly to the long axis with a waist of ≈ 10 mm. It homogeneously illuminates the cloud with Rabi frequencies $\Omega_p \lesssim 0.6$ MHz and detuning $\Delta_p = 80 \pm 20$ MHz from the $|e\rangle$ state to minimise its population. The coupling laser is derived from a frequency doubled Ti:Sa laser with a total power of 1.15 W focused to a waist of approximately $30 \mu\text{m}$ and is aligned collinearly with the long axis of the atom cloud for maximum homogeneity. In our measurements we keep the coupling Rabi frequency and the coupling laser detuning fixed to the values $\Omega_c \approx 27$ MHz, $\Delta_c = -77$ MHz and tune Ω_p and Δ_p . The combined linewidth of both lasers is $\lesssim 200$ kHz.

Our measurements are performed by varying the probe laser intensity over the range from 30 nW/cm^2 to $30 \mu\text{W/cm}^2$, which corresponds to Ω from 1.7 kHz to 56 kHz. The atom-light interaction time τ is set by suddenly switching an acousto-optical modulator for the probe laser while the coupling laser is continuously on. To account for the branching ratio for decay to the ground state or the shelving state $|s\rangle = |4s_{1/2}, F=1\rangle$ we scale the measured loss rates by a factor of two.

Reduction to an effective two-level description

The three-level system can be reduced to an effective two-level system with driving parameters Ω , Δ in the limit that the population in $|e\rangle$ is negligibly small, e.g. in the limit $|\delta_p| \approx |\delta_c| \gg \Omega_c \gg \Omega_p$. We assume the coupling laser creates dressed states of the form $|\tilde{e}\rangle \approx |e\rangle + \varepsilon|r\rangle$ and $|\tilde{r}\rangle \approx |r\rangle - \varepsilon|e\rangle$ with $\varepsilon = \Omega_c/(2|\delta_c|) \ll 1$. For $\delta_p \approx -\delta_c$ the excitation lasers couple the ground state $|g\rangle$ to the state $|\tilde{r}\rangle$ with an effective Rabi frequency $\Omega \approx \varepsilon\Omega_p$. For the lowest intensity data the measured scalings indicate the interactions have a negligible effect. Therefore we compare this data with master equation simulations in the non-interacting limit to calibrate the effective single-atom Rabi frequency (see Supplementary Text). We define the effective detuning Δ as the two-photon detuning from the

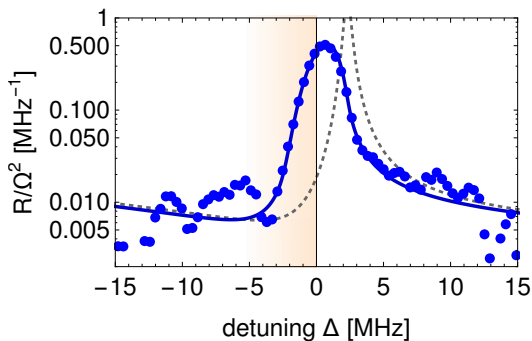


Figure S1. **Normalised loss rate as a function of detuning for the low intensity data.** The dotted line is the result of the single-atom master equation simulations. The solid line shows the theoretical spectrum including inhomogeneous broadening due to the atomic energy distribution in the optical trap. The shaded area represents the range of detunings corresponding to two-photon resonance including light shifts due to the optical trap.

$|g\rangle \rightarrow |\tilde{r}\rangle$ resonance at the center of the optical dipole trap $\Delta = \delta_p + \delta_c + \Delta_{\text{ODT}}$, where Δ_{ODT} accounts for the light shifts on the $|g\rangle \rightarrow |\tilde{r}\rangle$ transition due to the 1064 nm trap laser. However the position of maximum loss is additionally shifted by 0.5 MHz due to the AC Stark shift of the coupling laser and averaging over the inhomogeneous optical dipole potential. The effective excited state decay rate $\Gamma \approx \Gamma_r + \varepsilon^2 \Gamma_e \approx 100$ kHz is a combination of the bare Rydberg state decay $\Gamma_r \approx 1.2$ kHz (including blackbody transitions) and the residual intermediate state admixture which spontaneously decays with rate $\Gamma_e = 6.03$ MHz.

SUPPLEMENTARY INFORMATION

Model for the loss rate and its scaling in the non-interacting limit

In the limit where interactions are weak (i.e. the Rydberg population in the system is very small $\bar{N}\beta^2 \ll 1$) the dynamics of the system and Ω^2 scaling of the loss rate can be understood by single-particle theory. This condition is fulfilled in our experiments for the smallest values of Ω (cf. Fig. 4B) in both dissipation-dominated and driving-dominated regimes. Additionally the weak-driving data can be used to calibrate the effective Rabi

frequency Ω . To compare experiment and theory we solve the time-dependent quantum master equation describing coherent driving, spontaneous decay and optical pumping into the shelving state and model the loss of ground-state population in the experiment.

The master equation comprises the four-level atomic structure of ground state $|g\rangle = |4s_{1/2}, F=2, m_F=2\rangle$, intermediate state $|e\rangle = |4p_{3/2}\rangle$, Rydberg state $|r\rangle = |66s\rangle$ and shelving state $|s\rangle = |4s_{1/2}, F=1\rangle$. We use the atom-light Hamiltonian \hat{H} in the rotating wave approximation to describe the coherent coupling of $|g\rangle$, $|e\rangle$ and $|r\rangle$, while $|s\rangle$ is not coupled by any laser field. Furthermore, the superoperator $\mathcal{L}[\rho] = \sum_{\{\hat{L}\}} \hat{L}\rho\hat{L}^\dagger - (\hat{L}^\dagger\hat{L}\rho + \rho\hat{L}^\dagger\hat{L})/2$ describes dissipation due to spontaneous decay of the excited states, with a set of decay operators $\{\hat{L}\}$. We include decay operators which account for spontaneous decay from the Rydberg state to the intermediate state $\sqrt{\Gamma_r}|e\rangle\langle r|$ as well as from the intermediate state to both the ground and shelving states with equal probability $\sqrt{\Gamma_e/2}|g\rangle\langle e|$, $\sqrt{\Gamma_e/2}|s\rangle\langle e|$. The latter gives rise to the pumping of population into the shelving state. Additionally we include dephasing of the Rydberg state with a rate γ_{deph} by the operator $\sqrt{\gamma_{\text{deph}}}|r\rangle\langle r|$ which can account for the effects of laser linewidth and motion of the atoms. We then solve the time evolution of the density matrix $\dot{\rho}/(2\pi) = -(i/\hbar)[\hat{H}, \rho] + \mathcal{L}[\rho]$ and extract the population loss rate from the exponential decay of the ground state population in analogy to the experimental data analysis. In the limit $\Omega_p \ll \Gamma_e, \Omega_c$, as satisfied by the low-driving experiments, the loss rate scales proportionally to Ω_p^2 , as is shown in Figure 3 by the dotted lines.

To compare the simulation results with the experimental data we first scale the measured loss rates by Ω^2 (proportional to Ω_p^2) and average over the two lowest intensities to estimate the normalised loss rate in the noninteracting limit. This spectrum (Fig. S1) is significantly broader than can be explained from the solution of the quantum master equation outlined above. This is attributed to inhomogeneous level shifts mainly originating from the optical dipole trap. Therefore we convolve the simulated spectra by the energy distribution of atoms in the trap. Optimal agreement with the data is obtained for $\gamma_{\text{deph}} = 0.4$ MHz, $\Delta_{\text{ODT}} = 5.2$ MHz and $\sigma/w = 0.29$, where σ/w is the ratio of the cloud radius to the waist of the optical dipole trap. We use this measurement to calibrate the effective two photon Rabi frequency, which is within a factor of two of the theoretically expected value (see Methods).

-
- [1] R. Albert and A.-L. Barabási, Rev. Mod. Phys. **74**, 47 (2002).
 - [2] T. D. Lee and C. N. Yang, Phys. Rev. **87**, 410 (1952).
 - [3] H. Hinrichsen, Advances in physics **49**, 815 (2000).
 - [4] J. T. Barreiro, M. Müller, P. Schindler, D. Nigg, T. Monz, M. Chwalla, M. Hennrich, C. F. Roos, P. Zoller, and

- R. Blatt, Nature **470**, 486 (2011).
- [5] P. Schindler, M. Müller, D. Nigg, J. Barreiro, E. Martinez, M. Hennrich, T. Monz, S. Diehl, P. Zoller, and R. Blatt, Nature Physics **9**, 361 (2013).
- [6] J. G. Bohnet, B. C. Sawyer, J. W. Britton, M. L. Wall, A. M. Rey, M. Foss-feig, and J. J. Bollinger, Science **352**,

- 1297 (2016).
- [7] F. Brennecke, T. Donner, S. Ritter, T. Bourdel, M. Köhl, and T. Esslinger, *Nature* **450**, 268 (2007).
 - [8] Y. Colombe, T. Steinmetz, G. Dubois, F. Linke, D. Hunger, and J. Reichel, *Nature* **450**, 272 (2007).
 - [9] Y.-J. Lin, K. Jiménez-García, and I. Spielman, *Nature* **471**, 83 (2011).
 - [10] R. Landig, L. Hruby, N. Dogra, M. Landini, R. Mottl, T. Donner, and T. Esslinger, *Nature* **532**, 476 (2016).
 - [11] J. Kasprzak, M. Richard, S. Kundermann, A. Baas, P. Jeambrun, J. Keeling, F. Marchetti, M. Szymańska, R. Andre, J. Staehli, V. Savona, P. B. Littlewood, B. Deveaud, and L. S. Dang, *Nature* **443**, 409 (2006).
 - [12] C. Eichler, J. Mlynek, J. Butscher, P. Kurpiers, K. Hammerer, T. J. Osborne, and A. Wallraff, *Phys. Rev. X* **5**, 041044 (2015).
 - [13] H. Weimer, R. Löw, T. Pfau, and H. P. Büchler, *Phys. Rev. Lett.* **101**, 250601 (2008).
 - [14] P. Schauß, J. Zeiher, T. Fukuhara, S. Hild, M. Cheneau, T. Macrì, T. Pohl, I. Bloch, and C. Groß, *Science* **347**, 1455 (2015).
 - [15] H. Labuhn, D. Barredo, S. Ravets, S. de Léséleuc, T. Macrì, T. Lahaye, and A. Browaeys, *Nature* **534**, 667 (2016).
 - [16] R. Heidemann, U. Raitzsch, V. Bendkowsky, B. Butscher, R. Löw, L. Santos, and T. Pfau, *Physical Review Letters* **99**, 163601 (2007).
 - [17] R. Löw, H. Weimer, U. Krohn, R. Heidemann, V. Bendkowsky, B. Butscher, H. P. Büchler, and T. Pfau, *Phys. Rev. A* **80**, 033422 (2009).
 - [18] R. Löw, H. Weimer, J. Nipper, J. B. Balewski, B. Butscher, H. P. Büchler, and T. Pfau, *Journal of Physics B: Atomic, Molecular and Optical Physics* **45**, 113001 (2012).
 - [19] N. Henkel, R. Nath, and T. Pohl, *Phys. Rev. Lett.* **104**, 195302 (2010).
 - [20] F. Cinti, P. Jain, M. Boninsegni, A. Micheli, P. Zoller, and G. Pupillo, *Phys. Rev. Lett.* **105**, 135301 (2010).
 - [21] G. Pupillo, A. Micheli, M. Boninsegni, I. Lesanovsky, and P. Zoller, *Phys. Rev. Lett.* **104**, 223002 (2010).
 - [22] J. Honer, H. Weimer, T. Pfau, and H. P. Büchler, *Phys. Rev. Lett.* **105**, 160404 (2010).
 - [23] H. Schempp, G. Günter, M. Robert-de Saint-Vincent, C. S. Hofmann, D. Breyel, A. Komnik, D. W. Schönleber, M. Gärttner, J. Evers, S. Whitlock, and M. Weidemüller, *Phys. Rev. Lett.* **112**, 013002 (2014).
 - [24] N. Malossi, M. M. Valado, S. Scotto, P. Huillery, P. Pillet, D. Ciampini, E. Arimondo, and O. Morsch, *Phys. Rev. Lett.* **113**, 023006 (2014).
 - [25] A. Urvoy, F. Ripka, I. Lesanovsky, D. Booth, J. P. Shaffer, T. Pfau, and R. Löw, *Phys. Rev. Lett.* **114**, 203002 (2015).
 - [26] C. Simonelli, M. M. Valado, G. Masella, L. Asteria, E. Arimondo, D. Ciampini, and O. Morsch, *arXiv:1602.01257* (2016).
 - [27] C. Carr, R. Ritter, C. G. Wade, C. S. Adams, and K. J. Weatherill, *Phys. Rev. Lett.* **111**, 113901 (2013).
 - [28] N. Šibalić, C. G. Wade, C. S. Adams, K. J. Weatherill, and T. Pohl, *Phys. Rev. A* **94**, 011401 (2016).
 - [29] T. E. Lee, H. Häffner, and M. C. Cross, *Phys. Rev. Lett.* **108**, 023602 (2012).
 - [30] I. Lesanovsky and J. P. Garrahan, *Phys. Rev. Lett.* **111**, 215305 (2013).
 - [31] M. Hoening, W. Abdussalam, M. Fleischhauer, and T. Pohl, *Phys. Rev. A* **90**, 021603 (2014).
 - [32] R. Gutiérrez, J. P. Garrahan, and I. Lesanovsky, *Phys. Rev. E* **92**, 062144 (2015).
 - [33] M. Marcuzzi, M. Buchhold, S. Diehl, and I. Lesanovsky, *Phys. Rev. Lett.* **116**, 245701 (2016).
 - [34] J. Sanders, R. van Bijnen, E. Vredenbregt, and S. Kokkelmans, *Phys. Rev. Lett.* **112**, 163001 (2014).
 - [35] M. M. Valado, C. Simonelli, M. D. Hoogerland, I. Lesanovsky, J. P. Garrahan, E. Arimondo, D. Ciampini, and O. Morsch, *Phys. Rev. A* **93**, 040701 (2016).
 - [36] J. B. Balewski, A. T. Krupp, A. Gaj, S. Hofferberth, R. Löw, and T. Pfau, *New J. Phys.* **16**, 063012 (2014).
 - [37] E. A. Goldschmidt, T. Boulier, R. C. Brown, S. B. Koller, J. T. Young, A. V. Gorshkov, S. L. Rolston, and J. V. Porto, *Phys. Rev. Lett.* **116**, 113001 (2016).
 - [38] J. A. Aman, B. J. DeSalvo, F. B. Dunning, T. C. Killian, S. Yoshida, and J. Burgdörfer, *Phys. Rev. A* **93**, 043425 (2016).
 - [39] P. Schauß, M. Cheneau, M. Endres, T. Fukuhara, S. Hild, A. Omran, T. Pohl, C. Gross, S. Kuhr, and I. Bloch, *Nature* **491**, 87 (2012).
 - [40] G. Günter, H. Schempp, M. Robert-de Saint-Vincent, V. Gavryusev, S. Helmrich, C. S. Hofmann, S. Whitlock, and M. Weidemüller, *Science* **342**, 954 (2013).